NANO LETTERS

pubs.acs.org/NanoLett Letter

Shell-Free Copper Indium Sulfide Quantum Dots Induce Toxicity *in Vitro* and *in Vivo*

Joshua C. Kays, Alexander M. Saeboe, Reyhaneh Toufanian, Danielle E. Kurant, and Allison M. Dennis*

Cite This: https://dx.doi.org/10.1021/acs.nanolett.9b05259 Read Online

ABSTRACT: Semiconductor quantum dots (QDs) are attractive fluorescent contrast agents for *in vivo* imaging due to their superior photophysical properties, but traditional QDs comprise toxic materials such as cadmium or lead. Copper indium sulfide ($CuInS_2$, CIS) QDs have been posited as a nontoxic and potentially clinically translatable alternative; however, previous *in vivo* studies utilized particles with a passivating zinc sulfide (ZnS) shell, limiting direct evidence of the biocompatibility of the underlying CIS. For the first time, we assess the biodistribution and toxicity of unshelled CIS and partially zinc-alloyed CISZ QDs in a murine model. We show that bare CIS QDs breakdown quickly, inducing significant toxicity as seen in organ weight, blood chemistry, and histology. CISZ demonstrates significant, but lower, toxicity compared to bare CIS, while our measurements of core/shell CIS/ZnS are consistent with literature reports of general biocompatibility. *In vitro* cytotoxicity is dose-dependent on the amount of metal released due to particle degradation, linking degradation to toxicity. These results challenge the assumption that removing heavy metals necessarily reduces toxicity: indeed, we find comparable *in vitro* cytotoxicity between CIS and CdSe QDs, while CIS caused severe toxicity *in vivo* compared to CdSe. In addition to highlighting the complexity of nanotoxicity and the differences between the *in vitro* and *in vivo* outcomes, these unexpected results serve as a reminder of the importance of assessing the biocompatibility of core QDs absent the protective ZnS shell when making specific claims of compositional biocompatibility.

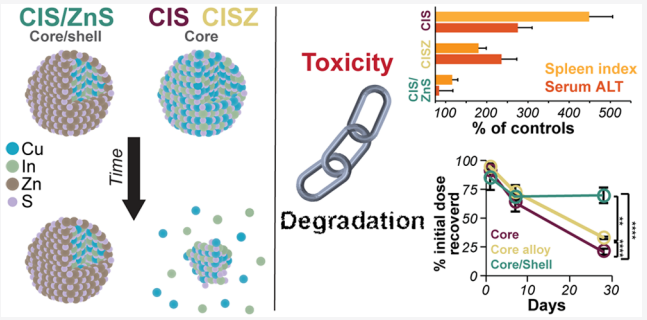

KEYWORDS: *QDs, nanotoxicity, CIS, $CuInS_2$, nanomedicine, in vivo imaging, biodegradable, fluorescent contrast agent*

Fluorescence imaging is a powerful diagnostic tool in both clinical and research settings due to the high spatial and temporal resolution of optical imaging as well as its safety and cost-effectiveness compared to ionizing radiation (X-rays and γ-rays).[1−3] In particular, near-infrared (NIR) imaging reduces the tissue scattering of visible light while avoiding attenuation from water absorption at longer wavelengths, permitting deeper tissue penetration.[1−3] The dearth of effective NIR emitters exhibiting ideal photophysical, chemical, and biocompatibility profiles, however, has limited broader clinical adoption of the technique. Semiconductor quantum dots (QDs) offer many advantages compared to standard organic dyes given their brightness, photostability, narrow and tunable photoluminescence (PL) peaks (allowing for multiplexing), and facile surface functionalization.[4,5] Furthermore, NIR-emitting QDs have already been used as powerful preclinical imaging agents *in vivo* with imaging depths of up to millimeters through tissue.[2]

NIR-emitting QDs have historically comprised toxic heavy metals such as lead, arsenic, cadmium, and mercury,[1] thus preventing clinical translation. Copper indium sulfide ($CuInS_2$, CIS) has emerged as a promising alternative due to its heavy-metal-free composition and NIR PL, which can be tuned from 500 to 950 nm by varying the Cu/In ratio.[6−8] CIS QDs capped with a ZnS shell (CIS/ZnS) reach photoluminescent quantum yields (QY) of up to 86% and can be effectively transferred into aqueous media, facilitating use in biomedical imaging applications.[9−11] The ZnS shell passivates trap states that can quench fluorescence and acts as an insulating layer to electron-withdrawing groups (OH in water).[12] ZnS shelling is ubiquitous across many QD systems due to its large band gap and ease of synthesis.[13] CIS/ZnS core/shell QDs have been tested *in vivo* in murine models for whole body imaging,[14] targeted tumor imaging,[6,15,16] and lymph node imaging;[17,18] these studies and more[11,19−21] have described CIS/ZnS QDs as "nontoxic," typically based on gross observation and histology. These successes and the elimination of the most concerning heavy metals from the particle composition have led researchers to claim that CIS QDs may have potential for clinical translation, for example in tumor imaging.[6,16,22]

Received: December 22, 2019
Revised: January 29, 2020
Published: January 30, 2020

https://dx.doi.org/10.1021/acs.nanolett.9b05259
Nano Lett. XXXX, XXX, XXX−XXX

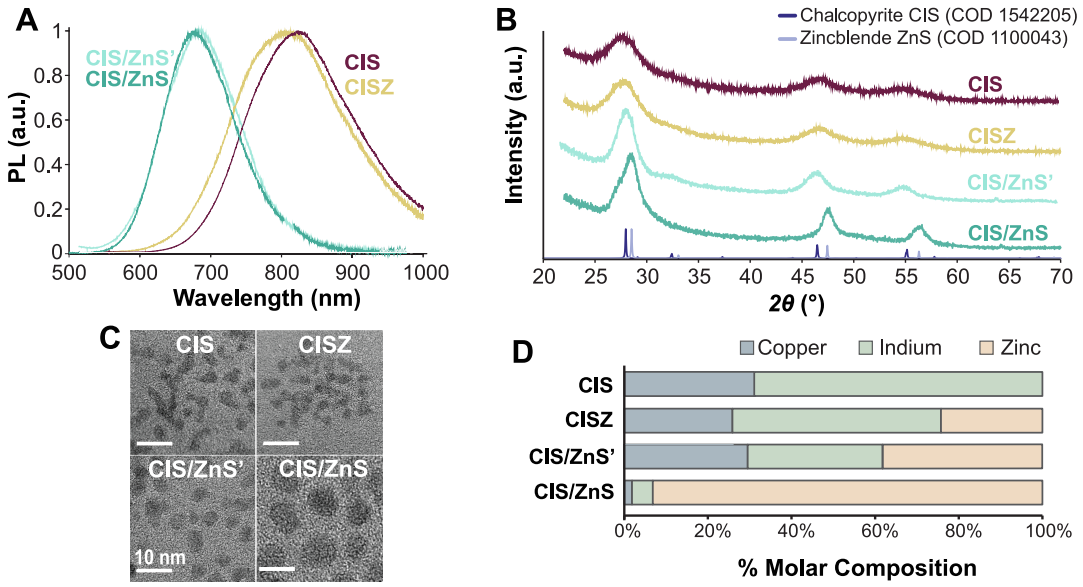

Figure 1. Characterization of CIS QDs. (A) Normalized photoluminescence (PL) spectra of CIS, zinc-treated CIS (CISZ), thin-shelled CIS (CIS/ZnS′), and thick-shelled CIS (CIS/ZnS). (B) X-ray diffraction (XRD) profiles of each QD type, along with reference peaks from the Crystallography Open Database (COD). The slight shift of the CIS/ZnS peaks corresponds to the growth of a solid ZnS shell (see reference peaks), while the decreased peak width indicates larger crystals, correlating with the TEM images. CIS and CISZ exhibit nearly identical peak positions. (C) Representative transmission electron microscopy (TEM) images of each QD. The scale bar is 10 nm. (D) Molar ratio of metal components of each QD, as determined by microwave plasma atomic emission spectroscopy (MP-AES).

However, studies have repeatedly demonstrated that ZnS shells render toxic QD core materials (such as CdSe and PbS) "nontoxic" *in vitro* and *in vivo*.[23−25] These and additional studies[26] document the significant accumulation of ZnS-shelled QDs with little to no clearance after months to years, including in monkeys.[25] These data fit the proposed mechanism that ZnS shells render toxic QD systems safe by preventing the degradation of the particle, trapping toxic ions,[27] and preventing reactive oxygen species (ROS) formation.[28] The lack of clearance from the body presents a significant hurdle to clinical translation. Of the ∼50 FDA-approved (United States Food and Drug Administration) nanomedicines available today,[29] all comprise biodegradable materials that are cleared from the body. The only inorganic FDA-approved nanoparticles comprise iron oxide, which biodegrades and is excreted through the biliary pathway, eliminating concerns of long-term toxicity. From the above, it seems unlikely that ZnS-capped QDs that bioaccumulate will receive serious consideration for clinical translation as diagnostic imaging agents, regardless of their exceptional optical properties or heavy-metal-free composition. Identifying degradable, nontoxic semiconductor materials could provide an alternative to the accumulation of ZnS-capped QDs. In this context, we sought to establish the biodegradation and biocompatibility of bare CIS QDs and zinc-treated CIS (i.e., CISZ) with comparison to the standard CIS/ZnS QDs.

There is a surprising dearth of literature on bare CIS particles in biological settings. We know of no studies of CIS stability or toxicity in mammals absent the ZnS shell. *In vitro*, a very recent study showed that CIS QDs can act as an immunomodulating agent on THP-1-derived macrophages, hindering pathogen clearance; CIS QDs appeared to be only mildly toxic at the highest doses tested (64 μM).[30] An additional *in vitro* study tested the cytotoxicity of hyaluronic acid-CIS nanorod clusters (∼100 nm) on B16F1 mouse melanoma cells, human erythroleukemia cells (HEL), and zebrafish embryos, showing little toxicity, though they did not test bare CIS nanorods separately.[31] No cytotoxicity studies of bare CIS QDs have been performed on standard cell lines or any primary human cells. A lone study of CIS stability and toxicity in *C. elegans* used CIS cores clustered together with carboxylated chitosan into 100−200 nm diameter particles.[32] This report found no cytotoxicity or *in vivo* toxicity from these particles, noting that "the extreme chemical stability of CIS QDs may explain the low cytotoxicity in the organism."[32] Importantly, the noted chemical stability is of the chitosan-embedded clusters, not of the bare CIS specifically. Our experiments, in contrast, are designed to observe the degradation and biocompatibility of bare QDs as micelle-encapsulated single particles.

In vitro, we observe the degradation of CIS and CISZ in a synthetic biological fluid, while CIS/ZnS QDs are stable. Using a murine model, we examine the *in vivo* biodistribution and toxicity of CIS particles at three time points (1, 7, and 28 days). CIS QDs are cleared relatively quickly, with <25% of the dose remaining in key organs (liver, spleen, kidneys, lungs, and heart) after one month. Surprisingly, we observe a significant toxic response to these QDs in measurements of organ mass, blood chemistry, and histology, which stands in stark contrast to previous literature on ZnS-shelled CIS.[6,7,10,11,14−16,18,33,34] Specifically, we find that a moderate dose (15 mg/kg) of CIS particles induces severe hepatotoxicity and splenotoxicity, with blood chemistry values indicating hepatic shock. CIS particles alloyed with zinc (CISZ QDs) demonstrate lower, but still significant, toxicity compared to bare CIS QDs, while CIS/ZnS generally show the least toxicity. Our *in vitro* cytotoxicity experiments demonstrate that partially degraded CIS particles impact cell viability at lower concentrations than intact CIS particles, indicating that the release of the CIS constituents plays a significant role in the toxic impact of the materials. Furthermore, we contextualized these results against cadmium selenide in both *in vitro* and *in vivo* experiments and found that

https://dx.doi.org/10.1021/acs.nanolett.9b05259
Nano Lett. XXXX, XXX, XXX−XXX

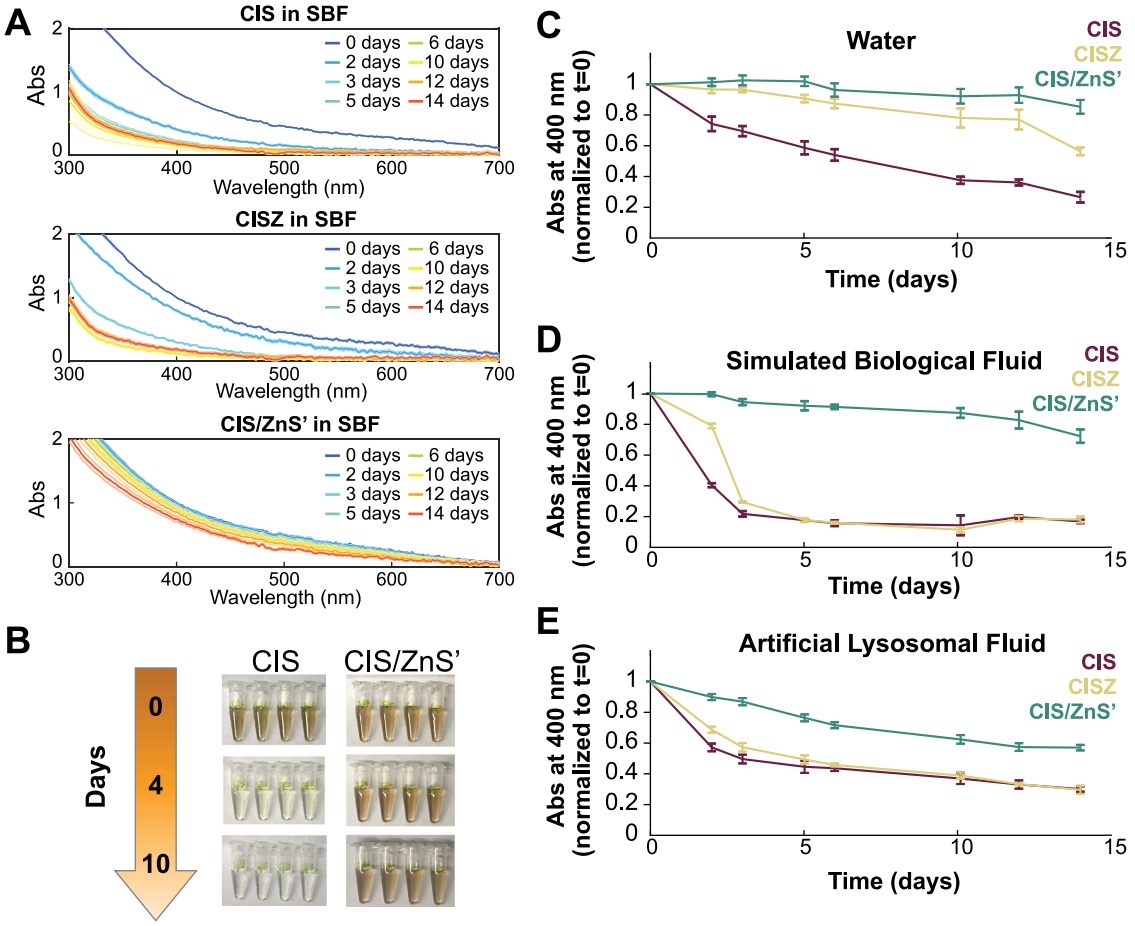

Figure 2. *In vitro* dissolution of CIS-based QDs. (A) Absorption spectra (mean ± standard deviation, $n = 4$) of micelle-encapsulated CIS, CISZ, and CIS/ZnS in a simulated biological fluid (SBF). Both CIS and CISZ degrade rapidly, while CIS/ZnS remains relatively stable. (B) Photos of CIS and CIS/ZnS solutions in SBF at days 1, 4, and 10. (C) Normalized absorbance at 400 nm of QDs in water, (D) SBF, and (E) artificial lysosomal fluid (ALF). CIS QDs dissolved in all solutions. CISZ exhibited similar dissolution kinetics to CIS in all solutions except water, while CIS/ZnS QDs were the most stable in all solutions. Mean ± standard deviation, $n = 4$.

bare CIS display similar *in vitro* cytotoxicity as bare CdSe cores and display far worse toxicity *in vivo* at the time point tested (7 days). These results act as a case study highlighting both the flaw in the assumption that QD biocompatibility will necessarily improve with the removal of traditional heavy metals (Cd, Pb) and the inherent complexity of nanomaterial toxicity *in vivo* and *in vitro*.

Copper indium sulfide QDs were initially synthesized via a heat-up method with a thiol precursor (dodecanethiol) as the sulfur source, as is typical in the field.[9,35,36] However, we found that these CIS cores and zinc-alloyed CIS (CISZ) QDs could not be encapsulated in a lipid-PEG micelle for water solubilization: only after adding a thin zinc sulfide shell (CIS/ZnS′), a procedure that introduces additional coordinating ligands, were these QDs successfully encapsulated. Thiol-based synthesis of CIS in octadecene (ODE) can lead to wrapping of the QDs in long-chain organic side products from a thiol−ene reaction,[37] potentially limiting interdigitation with the lipid-PEG during encapsulation. We switched to a thiol-free hot injection synthesis, modified from So et al.,[38] to circumvent this issue. CIS nanoparticles formed when the highly reactive sulfur precursor hexamethyldisilathiane was injected into a solution of copper and indium halide salts dissolved in trioctylphosphine (TOP) and ODE. Cleaned CIS cores were annealed with zinc stearate to incorporate zinc into the crystal structure, producing CISZ particles. Both CIS and CISZ QDs produced with the thiol-free approach formed stable micelles with lipid-PEG, as described below. CIS/ZnS core/shell particles for the biological experiments were synthesized according to a method previously tested *in vivo*:[17] in brief, cores were formed by the injection of bis(*N*-hexyldithiocarbamate) zinc ($Zn(NHDC)_2$) into a solution of $InCl_3$ and CuI in ODE, TOP, and oleylamine. To deposit a thick ZnS shell, $Zn(NHDC)_2$ and zinc stearate were dripped into heated, cleaned cores for 20 min. These particles were also then cleaned and encapsulated with lipid-PEG.

All of the QDs were characterized for their photophysical properties (Figure 1; Tables S1 and S2). Zinc alloying caused a slight blue shift in the fluorescence (from 822 nm for CIS to 808 nm for CISZ, Figure 1A), although transmission electron microscopy (TEM) indicates no change in size (3.5 ± 0.4 vs 3.4 ± 0.5 nm diameter). Elemental analysis with microwave plasma atomic energy spectroscopy (MP-AES) shows a 1/2.2 Cu/In ratio in the initial cores (from a 1/1 initial feed ratio) and a 1/1.9/0.9 Cu/In/Zn ratio in the CISZ particles; the Zn alloying replaced 17% of the Cu and 27% of the In atoms. The two different approaches to making the ZnS-shelled CIS described above yielded thin-shelled (CIS/ZnS′, 4.5 ± 0.8 nm diameter by TEM) and thick-shelled (CIS/ZnS, 10.5 ± 1.5 nm diameter by TEM) samples that emit at similar wavelengths

https://dx.doi.org/10.1021/acs.nanolett.9b05259
Nano Lett. XXXX, XXX, XXX−XXX

(681 and 676 nm, respectively). MP-AES results (1/1/1.3 vs 1/2.7/51 Cu/In/Zn for thin and thick shells, respectively) confirm higher zinc content with increased shelling. The X-ray diffraction (XRD) peaks of CIS and CISZ are virtually identical and match the reference peaks for chalcopyrite CIS well (Figure 1C). In comparison, ZnS shelling causes a progressive peak shift toward the zinc sulfide reference peak (28.53°) with increased shell thickness. Applying the Scherrer equation to the peak positions/widths yields sizes consistent with the TEM data for the cores (Table S2).

Each of the particles stably transferred into aqueous media through encapsulation in an amphiphilic lipid-polymer (1,2-distearoyl-*sn*-glycero-3-phosphoethanolamine-*N*-[methoxy-(polyethylene glycol)-2000] (ammonium salt); DSPE-PEG_{2k}) micelle with a minor modification to a previously published protocol.[39] DSPE-PEG_{2k} is common in clinical liposomal formulations (such as Doxil) due to its biocompatibility and ability to increase circulation time by preventing protein adsorption.[40] In addition, DSPE-PEG_{2k} is used in preclinical settings as a coating for injectable nanoparticles including QDs and iron oxide nanoparticles.[40−44] Cleaned QDs and DSPE-PEG_{2k} were mixed in chloroform, dried to a film with rotary evaporation, and resuspended in ultrapure water. Dynamic light scattering (DLS) demonstrates that all of the measured samples exhibit hydrodynamic diameters between 17 and 26 nm (Figure S1, Table S3), and negative-stained TEM of QD-micelles generally indicates the encapsulation of a single QD per micelle (Figure S2).

After characterizing and confirming the differences between these three particle types, we simulated *in vivo* degradation through an *in vitro* dissolution assay. For other nanoparticle systems, *in vitro* dissolution assays have proven to be a cost-effective way to compare different particle types and materials without using animals.[45−47] We compared two simulated physiological fluids alongside water: artificial lysosomal fluid (ALF, pH 4.5; recipe in Supporting Information) and simulated biological fluid (SBF, pH 7.3; recipe in Supporting Information). ALF is designed to imitate the composition and pH of macrophage lysosomes,[45,46] while SBF mimics the ionicity and pH of human blood plasma (Table S4).[48]

Encapsulated CIS, CISZ, and CIS/ZnS′ QDs were syringe filtered (0.1 μm), added to the three test solutions at similar optical densities, incubated at 45 °C, and monitored via UV−vis spectroscopy. QD absorbance decreased over time for CIS and CISZ, as shown in Figure 2A for SBF solutions (and observed visually, Figure 2B), with blue shifting of the band edge indicating shrinking particle diameter and particle dissolution (Figure S3). In all cases, CIS/ZnS′ absorbance was far more stable than CIS and CISZ, confirming the protective quality of ZnS shelling. CIS and CISZ exhibited nearly identical degradation profiles in both SBF and ALF, while CISZ was more stable in water compared to CIS. These results motivated the testing of the biodegradation and biocompatibility of CIS and CISZ particles *in vivo* to assess their potential as clinically relevant contrast agents with comparison to ZnS-shelled CIS at three time points: 1, 7, and 28 days postinjection.

To assess the degradation and biocompatibility of CIS QDs, BALB/cJ mice received tail vein intravenous (IV) injections of DSPE-PEG_{2k}-encapsulated QDs in sterile, endotoxin-free 0.9% saline. As stated above, DSPE-PEG_{2k} is a clinically approved excipient for several IV drugs and is frequently used as a neutrally charged nanoparticle coating to reduce or eliminate opsonization.[40,49] Indeed, ζ-potential measurements hovered around 0 mV (Table S5). For the *in vivo* studies, a dose of 15 mg/kg total cation content (based on elemental analysis, see Table 1) was selected, since it is within range of similarly tested QDs[34,50,51] and the clinical dosing range for the iron oxide nanoparticle injection Feraheme (7.3 mg/kg, assuming a 70 kg adult).[52] Control mice were injected with 0.9% saline vehicle, prepared under identical conditions and handling. For all of the biological experiments described below, we used the thicker-shelled CIS/ZnS samples as the thick ZnS shell is believed to provide improved stability and biocompatibility. Furthermore, this specific synthesis of thick-shelled CIS/ZnS particles has already been tested *in vivo* (albeit with a slightly different PEGylated micelle coating),[33] providing a helpful benchmark for our results.

Table 1. Injected Dose of QDs

QD	dose (total cation (metals) basis; mg/kg)[a]	elemental dose Cu (mg/kg)	In (mg/kg)	Zn (mg/kg)
CIS	14.9 (19.6)	2.3	12.6	0
CISZ	14.9 (20.1)	2.6	9.3	2.9
CIS/ZnS	12.5 (18.5)	0.2	0.8	11.5
CIS (UbiQD)	8.3 (11.0)	1.8	6.5	0
CIS/ZnS (UbiQD)	6.1 (8.8)	0.5	1.4	4.2
QD	dose (total metals basis; mg/kg)[b]	Cd (mg/kg)		Se (mg/kg)
CdSe	14.6	8.6		6.1

[a]The dose of Cu, In, and Zn injected on a mg/kg basis calculated from elemental analysis of samples. Sulfur not assessed by elemental analysis; value in parentheses includes calculated sulfur content assuming a 1/1 atomic ratio of cations and anions (i.e., 1/1 (Cu+In +Zn)/S). Values reported here are averages for each particle type. Careful notes of specific volume and concentration of particles injected into each animal were tracked, and the mouse-specific values were used for initial dose-based calculations of biodistribution. [b]The total dose of Cd and Se injected on a mg/kg basis using the measured Cd concentration and mathematically adding Se, assuming a 1/1 Cd/Se atomic ratio.

We assessed the persistence of CIS, CISZ, and CIS/ZnS in the liver, spleen, heart, lungs, and kidneys by acid digesting each organ and performing MP-AES for elemental analysis (Figure 3). The brain was also collected, but no indium was detected at any time (data not shown). All three particle types exhibit similar degradation profiles to each other on days 1 and 7. On day 28, however, CIS/ZnS exhibits the same total QD persistence as it had on day 7, while CIS and CISZ each show a significant decrease in material present at day 28, with the amount of material found by elemental analysis to depend on particle type: CIS/ZnS > CISZ > CIS (Figure 3B). At day 28, 70% of the initial dose of the CIS/ZnS was recovered, while only an average of 21% and 33% of the injected dose of CIS and CISZ was recovered, respectively. For CIS and CISZ, the persistence of the injected doses of indium and copper is very similar (Figure S4); there is no evidence of one ion becoming preferentially trapped in the tissue or leaching out of an intact particle for more rapid excretion.

Multiple *in vivo* QD studies have reported QDs persisting in vital organs for weeks postinjection, similar to our observations of CIS/ZnS QDs. Su et al. observed little change in total QD content in the liver 15 days and 80 days postinjection of CdTe

https://dx.doi.org/10.1021/acs.nanolett.9b05259
Nano Lett. XXXX, XXX, XXX−XXX

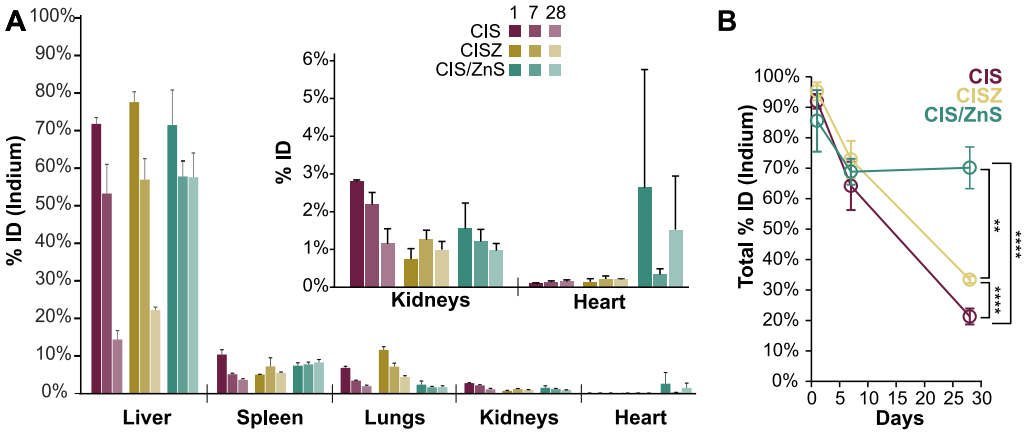

Figure 3. Biodistribution and clearance of CIS QDs. (A) Organ-specific distribution of indium over time (as % initial dose). Inset shows kidney and heart data on a different scale. (B) The summed indium content for CIS, CISZ, and CIS/ZnS. Asterisks indicate the significance level of comparison at day 28, as determined the Games-Howell ANOVA posthoc test: **, $p < 0.01$; ***, $p < 0.005$; ****, $p < 0.001$; $n = 4$. Error bars are one standard deviation.

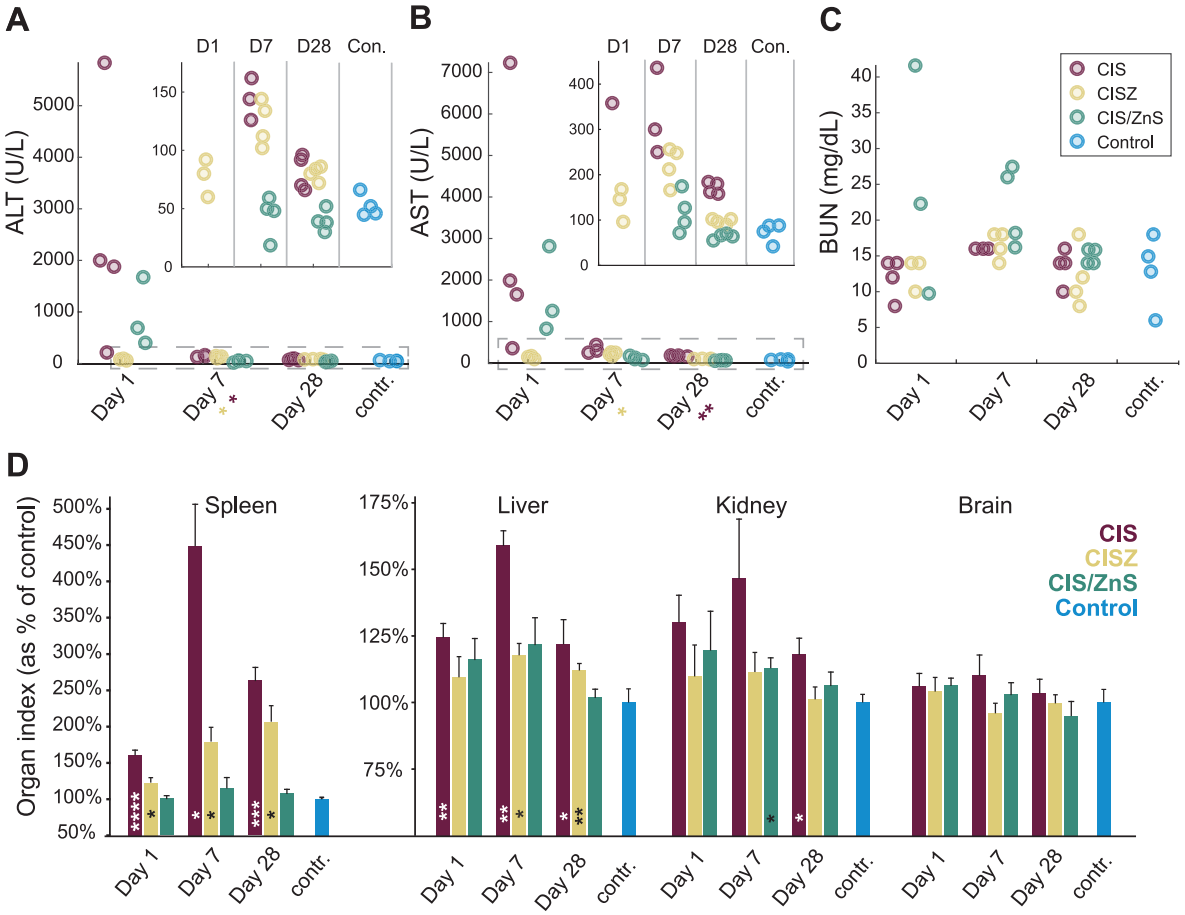

Figure 4. Blood biochemistry values. (A) ALT, (B) AST, and (C) BUN values for each animal. Insets are zoomed-in regions from dotted rectangles. (D) Organ index (organ weight/total body weight) plotted as the percent of control values for four major organs. Error bars are one standard deviation. Asterisks indicate the significance level compared to controls, as determined by the Games-Howell ANOVA posthoc test: *, $p < 0.05$; **, $p < 0.01$; ***, $p < 0.005$; ****, $p < 0.001$; $n = 4$ in all but two groups for organ index (CIS/ZnS D1 and CIS D7) and three groups for blood biochemistry (CISZ D1, CIS/ZnS D1, and CIS D7), which were $n = 3$. Note the different organ index axis scaling for the spleen compared to the other organs.

QDs.[26] Similarly, Hauck et al. demonstrated no change in the spleen and liver content of CdSe/ZnS QDs between days 3 and 30, with 30−50% of the peak Cd content remaining at day 112.[23] Among cadmium-free systems, Yaghini et al. tested InP/ZnS QDs *in vivo*, finding that ~50% of the peak dose remained at 30 days and 25−30% of the peak remained at the longest tested time point (90 days).[51] A recent report from Zou et al., the first to describe the biodistribution of IV injected CIS/ZnS QDs, shows a large drop in QD content between day 3 and day 30, but also notes the persistence of indium (and QD

https://dx.doi.org/10.1021/acs.nanolett.9b05259
Nano Lett. XXXX, XXX, XXX−XXX

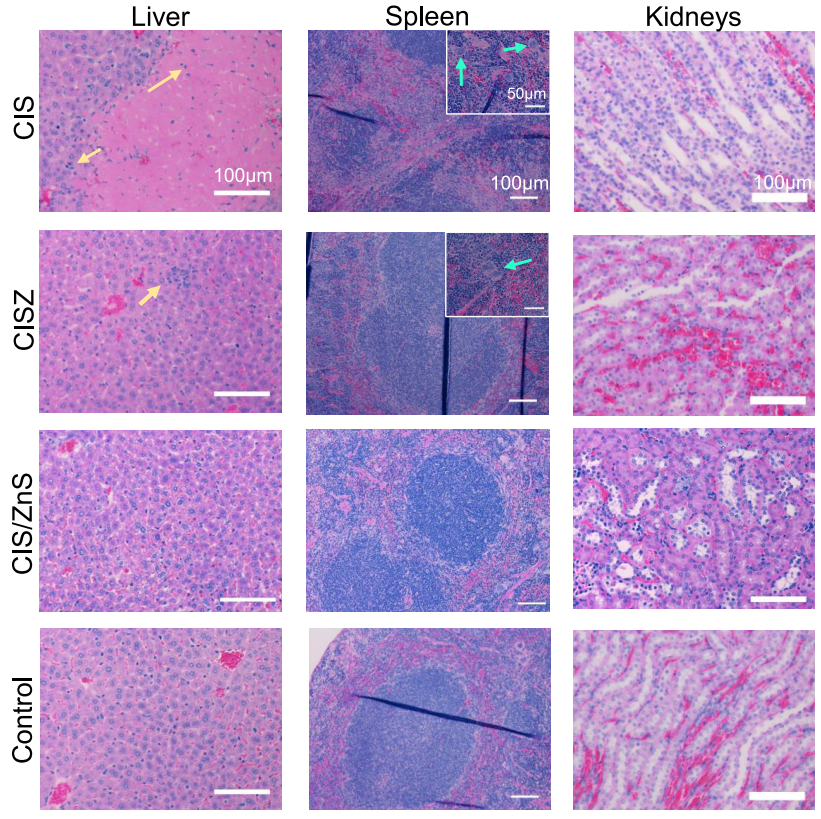

Figure 5. Histology of QD-dosed mice. Left, middle, and right columns show liver, spleen, and kidney, respectively. Yellow arrows indicate inflammatory cells; blue arrows point to multinucleated giant cells. The scale bar is 100 μm for primary photos and 50 μm for inserts.

fluorescence) in vital organs for up to 90 days.[34] Multiple long-term biodistribution studies of ZnS-shelled QD show slow (>50% of day 1 content remaining) to no clearance after a month across multiple compositions.[23,25,26,51,53−56] These long persistence times are consistent with our CIS/ZnS results and contrast with the rapid clearance of CIS and CISZ (Figure 3B).

We examined the *in vivo* toxicity of CIS, CISZ, and CIS/ZnS QDs in the same animals used in the biodistribution study by collecting a terminal blood draw for hematotoxicity and blood chemistry assays and recording organ indexes (organ weight/body weight) before organs were digested for metal content. Both CIS and CISZ show significant toxicity compared to controls at several time points in multiple metrics (Figure 4). CISZ exhibit elevated levels of both aspartate aminotransferase (AST) and alanine aminotransferase (ALT) at day 7, while CIS display statistically elevated AST at day 28 and ALT at day 7 (Figure 4A,B, Welch's ANOVA with Games-Howell posthoc test). The toxicity at day 1 for CIS QDs is particularly severe with values 4−110 times (ALT) or 5−99 times (AST) the control values, but the high variability in our data set limits determination of statistical significance. The AST and ALT values trend lower for CISZ compared to CIS at all time points; statistically, however, there are no differences between CISZ and CIS at most time points. Interestingly, hematotoxicity panels come back healthy for nearly all parameters at all time points for CIS and CISZ (Figure S5). At days 7 and 28, AST and ALT values for CIS/ZnS are statistically identical to controls (p = 0.67−0.99) and lower than the results for CIS and CISZ (Figure 4A). For example, CIS and CISZ show elevated ALT (144 and 123 U/L at day 7) compared to CIS/ZnS (44 U/L at day 7, $p < 0.05$ for both). At day 1, results for CIS/ZnS yield high AST/ALT values similar to CIS; however, the subjects at this time point were three moribund mice selected for euthanasia from an 11-mouse cohort due to severe symptoms in accordance to Institutional Animal Care and Use Committee (IACUC) policy. CIS/ZnS mice showed significant variation in toxicity (see discussion below), and those that survived to later time points appeared healthy during the whole study and exhibit narrowly distributed AST and ALT levels similar to controls. Blood urea nitrogen (BUN) levels, often used as an indicator of kidney health, are statistically comparable to controls for all groups at all time points, although the CIS/ZnS values are at times a little higher and more variable than the others (Figure 4C). Total protein, calcium ion levels, and albumin levels are consistent with controls (Figure S6) for all three particle types, further indicating normal kidney function.

The organ index, defined as the organ weight divided by the total body weight, is a highly sensitive measure of toxicity that exhibits significant changes even before the appearance of histological changes[57] and is a commonly required assay across multiple regulatory agencies.[58] Figure 4D displays the organ index for four organs normalized to the control values (organ index values before normalization listed in Table S6). Liver and spleen data demonstrate significant increases in the organ index for both CIS and CISZ compared to controls at nearly all time points. For example, the spleens of CIS-dosed mice spike to 450% (and CISZ-dosed mice to 200%) compared to controls, indicating massive splenomegaly. Meanwhile, CIS/ZnS show no change in the spleen index compared to controls and show no statistical difference in the liver index (though it trends higher at early time points). CIS causes large increases (to a max of 159%) in the liver index at days 1, 7, and 28, while CISZ induces increases in the liver index (to a max of 118%) at

https://dx.doi.org/10.1021/acs.nanolett.9b05259
Nano Lett. XXXX, XXX, XXX−XXX

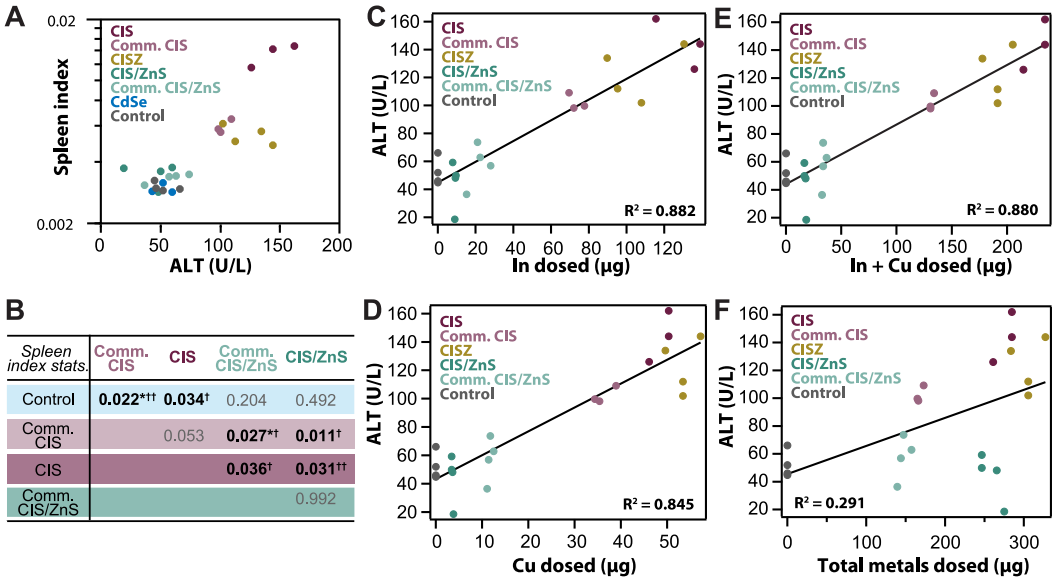

Figure 6. Comparative toxicity *in vivo*. (A) Spleen index (on a log scale) plotted against ALT values at day 7 for commercially sourced and lab-made CIS-based QDs as well as CdSe. (B) Results of the Games-Howell posthoc test for spleen index results. p values of pairwise comparisons are given in the table, with statistically significant values ($p < 0.05$) in bold type. Statistically significant pairwise comparisons of AST and ALT values are also marked with asterisks (*: $p < 0.05$) and daggers (†, $p < 0.05$; ††, $p < 0.01$), respectively. Plots of ALT versus (C) indium dose, (D) copper dose, (E) the sum of indium and copper dose, and (F) total cation dose (In + Cu + Zn) for individual mice, with linear fits included.

days 7 and 28. For context, murine models of alcoholism yield liver index increases to ∼133% of controls,[59] and the World Health Organization (WHO) guidelines for pesticide testing describe liver index changes of >15% (i.e., 115% increase by our terminology) as an adverse event.[60] Changes in kidney size are inconsistent: only CIS/ZnS and CIS show significant increases compared to controls, and each at only one time point (day 7 for CIS/ZnS and day 28 for CIS); other groups are elevated, compared to controls, but are too variable to be statistically significant.

To better understand the organ-specific toxicity of the CIS-based QDs, histopathology was performed on mice dosed at a slightly lower dose (12 mg/kg) and euthanized on day 3. The liver, spleen, and kidneys were fixed and stained with hematoxylin and eosin (H&E). Micrographs of these organs compared to control mice are presented in Figure 5. Geographic necrosis is seen throughout the liver of the CIS-dosed mice (consistent with liver marbling observed in gross dissection, Figure S7), along with significant cellular debris. Marked inflammation is noted in the livers of the CIS-dosed mice, whereas, in CISZ, the inflammation is mild, and no clear inflammation is seen in CIS/ZnS or control liver micrographs.

CIS spleens displayed the disruption of tissue architecture, along with apparent shrinkage of the white pulp and marginal zone expansion. In both CIS and CISZ spleens, multinucleated giant cells were present throughout (see inset), another indication of an inflammatory response. The inflammation is consistent with the significant splenomegaly seen for both CIS and CISZ QDs. Drug-induced splenomegaly typically has three root causes: direct harm to the spleen, hemolysis leading to higher filtration by the spleen, and/or liver damage, resulting in portal vein occlusion.[61] Given the disruption of spleen architecture as well as the severe liver damage, CIS QDs may be leading to direct spleen damage and/or indirect damage through liver toxicity, but further studies are necessary to elucidate the mechanism.

Interestingly, no significant histologic changes are noted in the kidneys of CIS, CISZ, or CIS/ZnS tested mice compared to controls. This seems to confirm the lack of kidney toxicity seen previously (Figures 4C, Figure S5). Generally, nanoparticles over 5 nm are cleared by the liver: multiple reports indicate that a primary mechanism of clearance is uptake by liver macrophages (e.g., Kupffer cells) followed by bile excretion.[62−64] Our evidence of QD dissolution in ALF and the low level of indium in the kidney digests (Figure 3) support this hypothesis. Future tracking of the excreted elements in feces and urine would confirm that this excretion route is prevalent in this instance as well.

The very high (and highly variable) levels of ALT and AST, along with the organ index and histopathology results, suggest severe heptatotoxicity to the point of ischemic hepatitis in the CIS-dosed mice.[65] Indeed, of the initial 13 mice injected with CIS QDs, 2 died between 24 and 96 h, and all CIS-injected mice displayed signs of toxicity, such as ruffled fur and lethargy. Furthermore, the liver is visibly marbled with fatty or necrotic tissue, compared to the control, CISZ-, and CIS/ZnS-injected mice (Figure S7). CISZ trends toward lower organ index changes than CIS for several organs, though only statistically significant at a few time points: the spleen exhibits a lower organ index in CISZ than CIS at day 1 ($p < 0.005$), as does the liver at day 7 ($p < 0.005$), potentially indicating lower toxicity of CISZ than CIS. This may be due to the reduced indium and copper content of CISZ compared to CIS, as dosing was determined by total metal content and not scaled to specific ions.

In general, our observations indicate that mice injected with CIS exhibit notable signs of stress and toxicity, which is milder for mice injected with CISZ, and largely absent for mice several days past their injections with CIS/ZnS. Multiple mice injected with CIS/ZnS did exhibit concerning signs of stress in the hours after the injection, however. These observations of stress were highly variable, despite dosing with identical materials. For example, in one experiment, 4 mice were injected with

https://dx.doi.org/10.1021/acs.nanolett.9b05259
Nano Lett. XXXX, XXX, XXX−XXX

identical doses from the same sterile tube of CIS/ZnS QDs in endotoxin-free saline, 0.1 μm filtered, loaded into sterile syringes, and delivered intravenously with no air bubbles. From this same tube, one mouse showed early signs of toxicity (reduced activity, reduced feeding) after 1 h and died before 14 h. Another mouse showed no signs of toxicity in the first 2 h but died before 14 h. The other two mice showed no gross toxicity, behaved normally, and lived throughout the course of the study. This surprising result from the CIS/ZnS injection prompted the testing of multiple complementary QD samples using the same lab, equipment, personnel, coating methods and reagents, etc. to validate our technique. Beyond the data discussed in this report, injections of comparable doses of QDs made in our lab comprising PbS/CdS or CdSe/ZnS coated with the same micelle-PEG (n = 3−4 for each composition) exhibited none of the morbidity or mortality we observed with our lab-made CIS and CIS/ZnS QDs (data not shown). In addition, commercially available CIS/ZnS QDs and custom-ordered CIS cores from the same company (UbiQD, Los Alamos, NM), as well as lab-made CdSe of comparable size (3.21 nm diameter, Figure S8), were tested at day 7 for comparison (discussion below, Figure 6). None of the same short-term morbidity seen in CIS/ZnS injections arose with the other cohorts of n = 4 mice injected with DSPE-PEG$_{2k}$-coated QDs.

Repeating our *in vivo* study at a single time point (day 7) using CIS and CIS/ZnS QDs manufactured by UbiQD, Inc., as well as lab-made CdSe cores, served to (1) test whether other preparations of CIS cores also induce a toxic response, (2) understand if the observed CIS/ZnS morbidity was synthesis-dependent, and (3) contextualize the results with a comparison to uncapped CdSe, which is generally accepted as toxic within the QD community. For this comparison, QDs were encapsulated in lipid-PEG identical to the CIS studies and were handled under identical conditions. At day 7, blood was collected, and mice were euthanized and organs harvested for organ index measurements and elemental analysis. The metal-basis dose of the CIS and CIS/ZnS particles was about half that of the lab-made samples, while CdSe was dosed at 15 mg/kg (Table 1).

As a whole, the results from the commercially sourced QDs validate our results (Figure 6). Commercial CIS cause elevated AST levels (mean 169 U/L), similar to CISZ and slightly below (but not statistically different from) our in-house CIS (p = 0.36). Similarly, spleen index and ALT values are greatly increased compared to controls, yet equivalent to our lab-made CIS (Figure 6B, Tables S6−9). In contrast, commercial CIS/ZnS did not recreate the sporadic toxicity we saw for our own CIS/ZnS: there were no deaths, no visible toxicity (behavior changes, fur appearance, or activity) nor measurable changes in AST, ALT, or organ index, compared to controls or compared to our later time point CIS/ZnS data. Despite exhibiting similar particle biodistribution to the CIS QDs (Figure S9), CdSe surprisingly shows no toxicity at this time point, yielding organ index and AST values similar to controls. CdSe is known to be cytotoxic due mainly to the release of Cd^{2+} ions and resultant DNA damage,[27,66−68] but few studies on bare CdSe QDs exist *in vivo*. To understand this lack of toxicity, the *in vitro* assay from Figure 2 was performed on CdSe QDs: we found no degradation with these specific QDs (Figure S10), which seems to explain the lack of toxicity we saw *in vivo* at this one time point and may be additional evidence linking degradation to toxicity (and the lack of degradation to *in vivo* dose tolerance). Additionally, discrepancies between *in vitro* and *in vivo* toxicity (with *in vitro* results being more toxic than *in vivo*) have been shown repeatedly for QDs.[69] Overall, these day 7 results confirmed that CIS is toxic, while CIS/ZnS is more biocompatible due to the masking effect of the ZnS shell.

Our dosing of multiple CIS compositions, with various doses and ion content, allows for aggregate analysis at the day 7 time point. For example, plotting the hydrodynamic particle diameter against the spleen index shows that there is no size dependence driving the toxicity of the particles (Figure S11). We test the relationship between composition and toxicity by plotting dosed metal content against biological metrics (Figure 6C−F). Specifically, plots of indium dosing and copper dosing vs ALT yield surprisingly high R^2 values (0.88 and 0.84, respectively). Though collinearity between indium and copper dosing precludes separating the contributions of each ion, their combined impact on ALT yields a strong correlation between dosing and toxicity (R^2 = 0.88, p < 0.0001). The inclusion of the zinc in the dosing parameter, in contrast, yields a poor fit to a linear model (Figure 6F).

The results of this *in vivo* analysis motivated an *in vitro* examination of cytotoxicity. Specifically, to better understand the mechanism of CIS toxicity, we measured the impact of CIS, partially degraded CIS, CISZ, CIS/ZnS, and CdSe on the human liver cancer cell line HepG2 (Figure 7). Cells were incubated in QD-containing media for 24 h, after which the media was aspirated, wells were washed with phosphate-buffered saline, and ATP levels were measured using a standard viability assay (CellTiter-Glo Luminescent Cell Viability Assay, Promega).

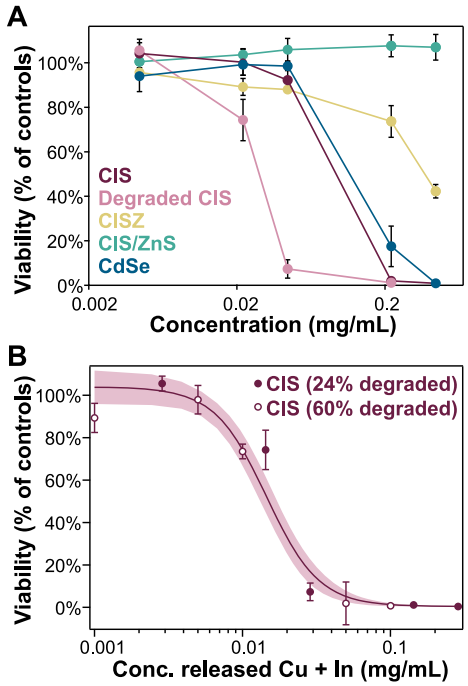

Figure 7. *In vitro* toxicity assay. (A) Quantification of HepG2 viability after 24 h treatment with QDs, n = 4 wells per dose. (B) Dose−response curve derived from viability assays for two levels of degradation fit to a 4-parameter Hill equation; shaded region indicates the 95% confidence interval.

A clear dose-dependent toxicity is seen for CIS, degraded CIS, and CdSe (Figure 7A). CdSe and intact CIS cause nearly

https://dx.doi.org/10.1021/acs.nanolett.9b05259
Nano Lett. XXXX, XXX, XXX−XXX

identical changes in viability at all doses tested, while CISZ shows reduced toxicity compared to CIS, and CIS/ZnS shows no toxicity at all doses tested, similar to our *in vivo* results. The striking similarity of cytotoxicity between bare CIS cores and CdSe, which is known to be cytotoxic,[66,67] challenges the assumption that removing heavy metals necessarily improves toxicity. The partially degraded CIS showed severe cytotoxicity at a dose 5-fold lower than CIS, linking degradation to toxicity. This link was additionally tested by treating cells with a more mildly degraded CIS (24% degraded vs 60% degraded with SBF vs acid, respectively; Figure S12), which results in a trend of increasing toxicity with increased degradation: CIS < 24% degraded CIS < 60% degraded CIS. The absorbance change for these predegraded CIS QDs was used to calculate the concentration of released CIS (Cu + In) for each of the doses in the cytotoxicity study. By combining the two data sets, we have 9 concentrations of released copper and indium, which yield a dose−response curve with an LC_{50} of ∼0.014 mg/mL (Figure 7B, χ^2 = 22.2). Combining the two data sets for a dose−response curve based on their intact particle concentration doses with the data for the intact particle dosing yields a much poorer fit (Figure S13, χ^2 = 219.9), potentially indicating cytotoxicity of CIS may be more related to the amount of degradation products than to the concentration of the intact particles themselves. Moreover, this link between degradation and toxicity *in vitro* may explain the severe toxicity seen for CIS *in vivo*.

The development of NIR-emitting QDs holds much promise for clinical and preclinical *in vivo* imaging; however, toxicity, heavy-metal content, and bioaccumulation in the RES have hindered translation.[22,70,71] New materials, such as CIS and AgS_2, may potentially alleviate these concerns, but most investigations of QD biocompatibility, including for CIS, use particles with protective ZnS shells that prevent degradation and leaching of core elements. These particles accumulate in essential organs, threatening clinical potential. To consider the true biocompatibility of the core material, it is critical to test the *in vivo* impact in the absence of the ZnS shell, since degradation and excretion *in vivo* are favorable for clinical translation.[72] We have demonstrated that bare CIS appears to degrade more quickly than other core QDs in the literature (e.g., CdSe and CdTe[26]) and much more quickly than ZnS-shelled QDs.[23,51] This rapid degradation of CIS appears concomitant with severe toxicity to the liver and spleen *in vivo*, and our *in vitro* assays link this increased degradation to increased toxicity. Zinc alloying lowers, but does not eliminate, the toxic response compared to controls. In both cases, the absence of a robust ZnS shell significantly altered the degradation and toxicological profile of the QDs. These results underscore two needs in the field: (1) rigorous toxicological evaluation of novel materials without confounding variables (such as the presence of an inert ZnS shell) and (2) re-evaluation of our assumptions regarding the relative safety and biocompatibility of heavy-metal-free materials.

■ ASSOCIATED CONTENT

Supporting Information

The Supporting Information is available free of charge at https://pubs.acs.org/doi/10.1021/acs.nanolett.9b05259.

Methods and materials, tables of further QD characterization data, demonstration of QD dissolution, organ weights and organ index values, figures of additional *in vivo* elemental analysis data, hematotoxicity assays, and more blood chemistry assays (PDF)

■ AUTHOR INFORMATION

Corresponding Author

Allison M. Dennis − *Department of Biomedical Engineering and Division of Materials Science & Engineering, Boston University, Boston, Massachusetts 02215, United States;* orcid.org/0000-0001-5759-9905; Email: aldennis@bu.edu

Authors

Joshua C. Kays − *Department of Biomedical Engineering, Boston University, Boston, Massachusetts 02215, United States*

Alexander M. Saeboe − *Division of Materials Science & Engineering, Boston University, Boston, Massachusetts 02215, United States*

Reyhaneh Toufanian − *Division of Materials Science & Engineering, Boston University, Boston, Massachusetts 02215, United States*

Danielle E. Kurant − *Department of Pathology, Brigham and Women's Hospital, Boston, Massachusetts 02115, United States*

Complete contact information is available at: https://pubs.acs.org/10.1021/acs.nanolett.9b05259

Author Contributions

J.C.K. and A.M.D. conceived of the project. J.C.K., A.M.S., R.T., and A.M.D. designed experiments. R.T. performed the synthesis and TEM experiments, J.C.K. and A.M.S. performed animal work. A.M.S. performed Hevamet experiments; all other experiments were performed by J.C.K. D.E.K performed histology analysis. J.C.K. and A.M.D. wrote the manuscript, and all authors have given approval to the final version of the manuscript.

Funding

The research reported in this publication was supported by the National Institute of General Medical Sciences of the National Institutes of Health under award number R01GM129437. Financial support for J.C.K. was provided by Training Grant NIH/NIGMS T32 GM008764 and by the National Science Foundation Graduate Research Fellowship (NSF-GRFP) under Grant No. DGE-1840990. Financial support for A.M.D. was provided by the National Center for Advancing Translational Sciences, National Institutes of Health, through BU-CTSI Grant Number 1KL2TR001411.

Notes

The authors declare no competing financial interest.

■ ACKNOWLEDGMENTS

XRD data was generated in the BU MSE Core Research Facility, funded by NSF Award Number 1337471. This work included services from the BUMC Experimental Pathology Laboratory Service Core. This work was accomplished by using instruments provided by the Boston University Analytical Instrumentation Core, and we specifically thank M. Au for his technical expertise in performing the hematology and chemical analyses. This work was performed in part at Harvard University's Center for Nanoscale Systems (CNS), a member of the National Nanotechnology Coordinated Infrastructure Network (NNCI), which is supported by the National Science Foundation under NSF award no. 1541959. We acknowledge the help of E. Upton of the MSSP statistical

https://dx.doi.org/10.1021/acs.nanolett.9b05259
Nano Lett. XXXX, XXX, XXX−XXX

consulting service at Boston University, under the guidance of M. Yajima, Ph.D.

■ ABBREVIATIONS LIST:

AgS_2: silver sulfide
ALF: artificial lysosomal fluid
ALT: alanine aminotransferase
AST: aspartate aminotransferase
BUN: blood urea nitrogen
CdSe: cadmium selenide
CdTe: cadmium telluride
CIS: copper indium sulfide
COD: crystallography open database
DLS: dynamic light scattering
DSPE-PEG: 1,2-distearoyl-*sn*-glycero-3-phosphoethanolamine-*N*-[methoxy(polyethylene glycol)
FDA: Food and Drug Administration
IACUC: institutional animal care and use committee
InP: indium phosphide
IV: intravenous
MP-AES: microwave plasma atomic emission spectroscopy
NIR: near-infrared
ODE: octadecene
PbS: lead sulfide
PL: photoluminescence
QD: quantum dot
ROS: reactive oxygen species
SBF: simulated biological fluid
TEM: transmission electron microscopy
TOP: trioctylphosphine
UV−vis: ultraviolet−visible
WHO: world health organization
XRD: X-ray diffraction
ZnS: zinc sulfide

■ REFERENCES

(1) Ma, Q.; Su, X. Near-Infrared Quantum Dots: Synthesis, Functionalization and Analytical Applications. *Analyst* **2010**, *135* (8), 1867.
(2) Zhang, M.; Yue, J.; Cui, R.; Ma, Z.; Wan, H.; Wang, F.; Zhu, S.; Zhou, Y.; Kuang, Y.; Zhong, Y.; et al. Bright Quantum Dots Emitting at ∼ 1,600 nm in the NIR-IIb Window for Deep Tissue Fluorescence Imaging. *Proc. Natl. Acad. Sci. U. S. A.* **2018**, *115* (26), 6590−6595.
(3) Hong, G.; Antaris, A. L.; Dai, H. Near-Infrared Fluorophores for Biomedical Imaging. *Nat. Biomed. Eng.* **2017**, *1* (1), 1.
(4) Medintz, I. L.; Uyeda, H. T.; Goldman, E. R.; Mattoussi, H. Quantum Dot Bioconjugates for Imaging, Labelling and Sensing. *Nat. Mater.* **2005**, *4* (6), 435−446.
(5) Bilan, R.; Fleury, F.; Nabiev, I.; Sukhanova, A. Quantum Dot Surface Chemistry and Functionalization for Cell Targeting and Imaging. *Bioconjugate Chem.* **2015**, *26* (4), 609−624.
(6) Deng, D.; Chen, Y.; Cao, J.; Tian, J.; Qian, Z.; Achilefu, S.; Gu, Y. High-Quality $CuInS_2$/ZnS Quantum Dots for in Vitro and in Vivo Bioimaging. *Chem. Mater.* **2012**, *24* (15), 3029−3037.
(7) Kim, Y. su; Lee, Y.; Kim, Y.; Kim, D.; Choi, H. S.; Park, J. C.; Nam, Y. S.; Jeon, D. Y. Synthesis of Efficient Near-Infrared-Emitting $CuInS_2$/ZnS Quantum Dots by Inhibiting Cation-Exchange for Bio Application. *RSC Adv.* **2017**, *7* (18), 10675−10682.
(8) Xie, R.; Rutherford, M.; Peng, X.; Fayette, V. Formation of High-Quality I - III - VI Semiconductor Nanocrystals by Tuning Relative Reactivity of Cationic Precursors. *J. Am. Chem. Soc.* **2009**, *131* (15), 5691−5697.
(9) Li, L.; Pandey, A.; Werder, D. J.; Khanal, B. P.; Pietryga, J. M.; Klimov, V. I. Efficient Synthesis of Highly Luminescent Copper Indium Sulfide-Based Core/Shell Nanocrystals with Surprisingly Long-Lived Emission. *J. Am. Chem. Soc.* **2011**, *133* (5), 1176−1179.
(10) Speranskaya, E. S.; Sevrin, C.; De Saeger, S.; Hens, Z.; Goryacheva, I. Y.; Grandfils, C. Synthesis of Hydrophilic $CuInS_2$/ZnS Quantum Dots with Different Polymeric Shells and Study of Their Cytotoxicity and Hemocompatibility. *ACS Appl. Mater. Interfaces* **2016**, *8* (12), 7613−7622.
(11) Kim, E. M.; Lim, S. T.; Sohn, M. H.; Jeong, H. J. Facile Synthesis of Near-Infrared $CuInS_2$/ZnS Quantum Dots and Glycol-Chitosan Coating for in Vivo Imaging. *J. Nanopart. Res.* **2017**, *19* (7), 1−12.
(12) Zhu, C. N.; Zheng, D. Y.; Cao, H. M.; Zhu, S. Y.; Liu, X. J. Aqueous Synthesis of Highly Fluorescent and Stable Cu-In-S/ZnS Core/Shell Nanocrystals for Cell Imaging. *RSC Adv.* **2017**, *7* (80), 51001−51007.
(13) Reiss, P.; Protière, M.; Li, L. Core/Shell Semiconductor Nanocrystals. *Small* **2009**, *5* (2), 154−168.
(14) Li, L.; Daou, T. J.; Texier, I.; Kim Chi, T. T.; Liem, N. Q.; Reiss, P. Highly Luminescent CuInS 2 /ZnS Core/Shell Nanocrystals: Cadmium-Free Quantum Dots for In Vivo Imaging. *Chem. Mater.* **2009**, *21* (12), 2422−2429.
(15) Yong, K. T.; Roy, I.; Hu, R.; Ding, H.; Cai, H.; Zhu, J.; Zhang, X.; Bergey, E. J.; Prasad, P. N. Synthesis of Ternary $CuInS_2$/ZnS Quantum Dot Bioconjugates and Their Applications for Targeted Cancer Bioimaging. *Integr. Biol.* **2010**, *2* (2−3), 121−129.
(16) Trapiella-Alfonso, L.; Pons, T.; Lequeux, N.; Leleu, L.; Grimaldi, J.; Tasso, M.; Oujagir, E.; Seguin, J.; D'Orlyé, F.; Girard, C.; et al. Clickable-Zwitterionic Copolymer Capped-Quantum Dots for in Vivo Fluorescence Tumor Imaging. *ACS Appl. Mater. Interfaces* **2018**, *10* (20), 17107−17116.
(17) Pons, T.; Pic, E.; Lequeux, N.; Cassette, E.; Bezdetnaya, L.; Guillemin, F.; Marchal, F.; Dubertret, B. Cadmium-Free $CuInS_2$/ZnS Quantum Dots for Sentinel Lymph Node Imaging with Reduced Toxicity. *ACS Nano* **2010**, *4* (5), 2531−2538.
(18) Helle, M.; Cassette, E.; Bezdetnaya, L.; Pons, T.; Leroux, A.; Plénat, F.; Guillemin, F.; Dubertret, B.; Marchal, F. Visualisation of Sentinel Lymph Node with Indium-Based near Infrared Emitting Quantum Dots in a Murine Metastatic Breast Cancer Model. *PLoS One* **2012**, *7* (8), e44433.
(19) Kolny-Olesiak, J.; Weller, H. Synthesis and Application of Colloidal $CuInS_2$ Semiconductor Nanocrystals. *ACS Appl. Mater. Interfaces* **2013**, *5* (23), 12221−12237.
(20) Macdonald, T. J.; Mange, Y. J.; Dewi, M.; McFadden, A.; Skinner, W. M.; Nann, T. Cation Exchange of Aqueous $CuInS_2$ Quantum Dots. *CrystEngComm* **2014**, *16* (40), 9455−9460.
(21) Long, X.; Zhang, F.; He, Y.; Hou, S.; Zhang, B.; Zou, G. Promising Anodic Electrochemiluminescence of Nontoxic Core/Shell $CuInS_2$/ZnS Nanocrystals in Aqueous Medium and Its Biosensing Potential. *Anal. Chem.* **2018**, *90* (5), 3563−3569.
(22) McHugh, K. J.; Jing, L.; Behrens, A. M.; Jayawardena, S.; Tang, W.; Gao, M.; Langer, R.; Jaklenec, A. Biocompatible Semiconductor Quantum Dots as Cancer Imaging Agents. *Adv. Mater.* **2018**, *30* (18), 1706356.
(23) Hauck, T. S.; Anderson, R. E.; Fischer, H. C.; Newbigging, S.; Chan, W. C. W. In Vivo Quantum-Dot Toxicity Assessment. *Small* **2010**, *6* (1), 138−144.
(24) Tang, Y.; Han, S.; Liu, H.; Chen, X.; Huang, L.; Li, X.; Zhang, J. The Role of Surface Chemistry in Determining In vivo Biodistribution and Toxicity of CdSe/ZnS Core-Shell Quantum Dots. *Biomaterials* **2013**, *34* (34), 8741−8755.
(25) Ye, L.; Yong, K. T.; Liu, L.; Roy, I.; Hu, R.; Zhu, J.; Cai, H.; Law, W. C.; Liu, J.; Wang, K.; et al. A Pilot Study in Non-Human Primates Shows No Adverse Response to Intravenous Injection of Quantum Dots. *Nat. Nanotechnol.* **2012**, *7* (7), 453−458.
(26) Su, Y.; Peng, F.; Jiang, Z.; Zhong, Y.; Lu, Y.; Jiang, X.; Huang, Q.; Fan, C.; Lee, S. T.; He, Y. In Vivo Distribution, Pharmacokinetics, and Toxicity of Aqueous Synthesized Cadmium-Containing Quantum Dots. *Biomaterials* **2011**, *32* (25), 5855−5862.

https://dx.doi.org/10.1021/acs.nanolett.9b05259
Nano Lett. XXXX, XXX, XXX−XXX

(27) Derfus, A. M.; Chan, W. C. W.; Bhatia, S. N. Probing the Cytotoxicity of Semiconductor Quantum Dots. *Nano Lett.* **2004**, *4* (1), 11−18.
(28) Ipe, B. I.; Lehnig, M.; Niemeyer, C. M. On the Generation of Free Radical Species from Quantum Dots. *Small* **2005**, *1* (7), 706−709.
(29) Bobo, D.; Robinson, K. J.; Islam, J.; Thurecht, K. J.; Corrie, S. R. Nanoparticle-Based Medicines: A Review of FDA-Approved Materials and Clinical Trials to Date. *Pharm. Res.* **2016**, *33* (10), 2373−2387.
(30) Yao, C. X.; Lin, T. Y.; Su, Y. L.; Zou, H.; Yan, Z. Y.; Wu, S. M. Inhibitory Effects of $CuInS_2$ and CdTe Nanoparticles on Macrophage Cytokine Production and Phagocytosis in Vitro. *Enzyme Microb. Technol.* **2019**, *127*, 50−57.
(31) Chen, S. H.; Huang, W. W.; Dehvari, K.; Ling, Y. C.; Ghule, A. V.; Tsai, S. L.; Chang, J. Y. Photosensitizer−Conjugated Cu-In-S Heterostructured Nanorods for Cancer Targeted Photothermal/Photodynamic Synergistic Therapy. *Mater. Sci. Eng., C* **2019**, *97*, 793−802.
(32) Chen, C. W.; Wu, D. Y.; Chan, Y. C.; Lin, C. C.; Chung, P. H.; Hsiao, M.; Liu, R. S. Evaluations of the Chemical Stability and Cytotoxicity of $CuInS_2$ and $CuInS_2$/ZnS Core/Shell Quantum Dots. *J. Phys. Chem. C* **2015**, *119* (5), 2852−2860.
(33) Pons, T.; Pic, E.; Lequeux, N.; Cassette, E.; Bezdetnaya, L.; Guillemin, F.; Marchal, F.; Dubertret, B. Cadmium-Free $CuInS_2$/ZnS Quantum Dots for Sentinel Lymph Node Imaging with Reduced Toxicity. *ACS Nano* **2010**, *4* (5), 2531−2538.
(34) Zou, W.; Li, L.; Chen, Y.; Chen, T.; Yang, Z.; Wang, J.; Liu, D.; Lin, G.; Wang, X. In Vivo Toxicity Evaluation of PEGylated $CuInS_2$/ZnS Quantum Dots in BALB/c Mice. *Front. Pharmacol.* **2019**, *10* (APR), 1−10.
(35) De Trizio, L.; Prato, M.; Genovese, A.; Casu, A.; Povia, M.; Simonutti, R.; Alcocer, M. J. P.; D'Andrea, C.; Tassone, F.; Manna, L. Strongly Fluorescent Quaternary Cu-In-Zn-S Nanocrystals Prepared from $Cu_{1-x}InS_2$ nanocrystals by Partial Cation Exchange. *Chem. Mater.* **2012**, *24* (12), 2400−2406.
(36) Xia, C.; Meeldijk, J. D.; Gerritsen, H. C.; De Mello Donega, C. Highly Luminescent Water-Dispersible NIR-Emitting Wurtzite $CuInS_2$/ZnS Core/Shell Colloidal Quantum Dots. *Chem. Mater.* **2017**, *29* (11), 4940−4951.
(37) Akdas, T.; Distaso, M.; Kuhri, S.; Winter, B.; Birajdar, B.; Spiecker, E.; Guldi, D. M.; Peukert, W. The Effects of Post-Processing on the Surface and the Optical Properties of Copper Indium Sulfide Quantum Dots. *J. Colloid Interface Sci.* **2015**, *445*, 337−347.
(38) So, D.; Konstantatos, G. Thiol-Free Synthesized Copper Indium Sulfide Nanocrystals as Optoelectronic Quantum Dot Solids. *Chem. Mater.* **2015**, *27* (24), 8424−8432.
(39) Hu, R.; Law, W. C.; Lin, G.; Ye, L.; Liu, J.; Liu, J.; Reynolds, J. L.; Yong, K. T. PEGylated Phospholipid Micelle-Encapsulated Near-Infrared PbS Quantum Dots for in Vitro and in Vivo Bioimaging. *Theranostics* **2012**, *2* (7), 723−733.
(40) Xiao, R.; Wang, R.; Zeng, Z.; Lili Xu; Wang, J. Application of Poly (Ethylene Glycol)−Distearoylphosphatidylethanolamine (PEG-DSPE) Block Copolymers and Their Derivatives as Nanomaterials in Drug Delivery. *Int. J. Nanomed.* **2012**, *7*, 4185.
(41) Dubertret, B.; Skourides, P.; Norris, D. J.; Noireaux, V.; Brivanlou, A. H.; Libchaber, A. In Vivo Imaging of Quantum Dots Encapsulated in Phosopholipid Micelles. *Science (Washington, DC, U. S.)* **2002**, *298* (5599), 1759−1762.
(42) Lee, S.; George Thomas, R.; Ju Moon, M.; Ju Park, H.; Park, I. K.; Lee, B. Il; Yeon Jeong, Y. Near-Infrared Heptamethine Cyanine Based Iron Oxide Nanoparticles for Tumor Targeted Multimodal Imaging and Photothermal Therapy. *Sci. Rep.* **2017**, *7* (1), 1−14.
(43) Liu, X.; Lin, X.; Wu, M.; Lin, R.; Li, B.; Liu, J. SPION@$Cu_{2-x}S$ Nanoclusters for Highly Sensitive MRI and Targeted Photothermal Therapy of Hepatocellular Carcinoma. *J. Mater. Chem. B* **2016**, *4* (23), 4119−4129.
(44) Che, J.; Okeke, C.; Hu, Z.-B.; Xu, J. DSPE-PEG: A Distinctive Component in Drug Delivery System. *Curr. Pharm. Des.* **2015**, *21*, 1598−1605.
(45) Stopford, W.; Turner, J.; Cappellini, D.; Brock, T. Bioaccessibility Testing of Cobalt Compounds. *J. Environ. Monit.* **2003**, *5* (4), 675−680.
(46) Stebounova, L. V.; Guio, E.; Grassian, V. H. Silver Nanoparticles in Simulated Biological Media: A Study of Aggregation, Sedimentation, and Dissolution. *J. Nanopart. Res.* **2011**, *13* (1), 233−244.
(47) Adamcakova-Dodd, A.; Stebounova, L. V.; Kim, J. S.; Vorrink, S. U.; Ault, A. P.; O'Shaughnessy, P. T.; Grassian, V. H.; Thorne, P. S. Toxicity Assessment of Zinc Oxide Nanoparticles Using Sub-Acute and Sub-Chronic Murine Inhalation Models. *Part. Fibre Toxicol.* **2014**, *11* (1), 15.
(48) Marques, M. R. C.; Loebenberg, R.; Almukainzi, M. Simulated Biological Fluids with Possible Application in Dissolution Testing. *Dissolution Technol.* **2011**, *18* (3), 15−28.
(49) Carion, O.; Mahler, B.; Pons, T.; Dubertret, B. Synthesis, Encapsulation, Purification and Coupling of Single Quantum Dots in Phospholipid Micelles for Their Use in Cellular and in Vivo Imaging. *Nat. Protoc.* **2007**, *2* (10), 2383−2390.
(50) Guo, L.; Panderi, I.; Yan, D. D.; Szulak, K.; Li, Y.; Chen, Y. T.; Ma, H.; Niesen, D. B.; Seeram, N.; Ahmed, A.; et al. A Comparative Study of Hollow Copper Sulfide Nanoparticles and Hollow Gold Nanospheres on Degradability and Toxicity. *ACS Nano* **2013**, *7* (10), 8780−8793.
(51) Yaghini, E.; Turner, H.; Pilling, A.; Naasani, I.; MacRobert, A. J. In Vivo Biodistribution and Toxicology Studies of Cadmium-Free Indium-Based Quantum Dot Nanoparticles in a Rat Model. *Nanomedicine* **2018**, *14*, 2644.
(52) AMAG Pharmaceuticals, I. Feraheme [prescribing information] https://www.feraheme.com/dosing-and-administration/.
(53) Fischer, H. C.; Liu, L.; Pang, K. S.; Chan, W. C. W. Pharmacokinetics of Nanoscale Quantum Dots: In Vivo Distribution, Sequestration, and Clearance in the Rat. *Adv. Funct. Mater.* **2006**, *16* (10), 1299−1305.
(54) Lin, G.; Ouyang, Q.; Hu, R.; Ding, Z.; Tian, J.; Yin, F.; Xu, G.; Chen, Q.; Wang, X.; Yong, K. T. In Vivo Toxicity Assessment of Non-Cadmium Quantum Dots in BALB/c Mice. *Nanomedicine* **2015**, *11* (2), 341−350.
(55) Yaghini, E.; Turner, H. D.; Le Marois, A. M.; Suhling, K.; Naasani, I.; MacRobert, A. J. In Vivo Biodistribution Studies and Ex Vivo Lymph Node Imaging Using Heavy Metal-Free Quantum Dots. *Biomaterials* **2016**, *104*, 182−191.
(56) Liu, N.; Mu, Y.; Chen, Y.; Sun, H.; Han, S.; Wang, M.; Wang, H.; Li, Y.; Xu, Q.; Huang, P.; et al. Degradation of Aqueous Synthesized CdTe/ZnS Quantum Dots in Mice: Differential Blood Kinetics and Biodistribution of Cadmium and Tellurium. *Part. Fibre Toxicol.* **2013**, *10* (1), 37.
(57) Piao, Y.; Liu, Y.; Xie, X. Change Trends of Organ Weight Background Data in Sprague Dawley Rats at Different Ages. *J. Toxicol. Pathol.* **2013**, *26* (1), 29−34.
(58) Michael, B.; Yano, B.; Sellers, R. S.; Perry, R.; Morton, D.; Roome, N.; Johnson, J. K.; Schafer, K. Evaluation of Organ Weights for Rodent and Non-Rodent Toxicity Studies: A Review of Regulatory Guidelines and a Survey of Current Practices. *Toxicol. Pathol.* **2007**, *35* (5), 742−750.
(59) Uesugi, T.; Froh, M.; Arteel, G. E.; Bradford, B. U.; Wheeler, M. D.; Gabele, E.; Isayama, F.; Thurman, R. G. Role of Lipopolysaccharide-Binding Protein in Early Alcohol-Induced Liver Injury in Mice. *J. Immunol.* **2002**, *168* (6), 2963−2969.
(60) World Health Organization. *Pesticide Residues in Food: WHO Core Assessment Group on Pesticide Residues: Guidance Document for WHO Monographers and Reviewers*; World Health Organization: Geneva, 2015.
(61) Petroianu, A. Drug-Induced Splenic Enlargement. *Expert Opin. Drug Saf.* **2007**, *6* (2), 199−206.

https://dx.doi.org/10.1021/acs.nanolett.9b05259
Nano Lett. XXXX, XXX, XXX−XXX

(62) Tsoi, K. M.; Macparland, S. A.; Ma, X. Z.; Spetzler, V. N.; Echeverri, J.; Ouyang, B.; Fadel, S. M.; Sykes, E. A.; Goldaracena, N.; Kaths, J. M.; et al. Mechanism of Hard-Nanomaterial Clearance by the Liver. *Nat. Mater.* **2016**, *15* (11), 1212−1221.
(63) Sun, J. Kupffer Cell-Mediated Hepatic Injury Induced by Silica Nanoparticles in Vitro and in Vivo. *Int. J. Nanomed.* **2013**, 1129−1140.
(64) Briley-Saebo, K.; Bjørnerud, A.; Grant, D.; Ahlstrom, H.; Berg, T.; Kindberg, G. M. Hepatic Cellular Distribution and Degradation of Iron Oxide Nanoparticles Following Single Intravenous Injection in Rats: Implications for Magnetic Resonance Imaging. *Cell Tissue Res.* **2004**, *316* (3), 315−323.
(65) Raurich, J. M.; Pérez, O.; Llompart-Pou, J. A.; Ibáñez, J.; Ayestarán, I.; Pérez-Bárcena, J. Incidence and Outcome of Ischemic Hepatitis Complicating Septic Shock. *Hepatol. Res.* **2009**, *39* (7), 700−705.
(66) Oh, E.; Liu, R.; Nel, A.; Gemill, K. B.; Bilal, M.; Cohen, Y.; Medintz, I. L. Meta-Analysis of Cellular Toxicity for Cadmium-Containing Quantum Dots. *Nat. Nanotechnol.* **2016**, *11* (5), 479−486.
(67) Bilal, M.; Oh, E.; Liu, R.; Breger, J. C.; Medintz, I. L.; Cohen, Y. Toxicity Models: Bayesian Network Resource for Meta-Analysis: Cellular Toxicity of Quantum Dots (Small 34/2019). *Small* **2019**, *15* (34), 1970181.
(68) Atha, D. H.; Nagy, A.; Steinbrück, A.; Dennis, A. M.; Hollingsworth, J. A.; Dua, V.; Iyer, R.; Nelson, B. C. Quantifying Engineered Nanomaterial Toxicity: Comparison of Common Cytotoxicity and Gene Expression Measurements. *J. Nanobiotechnol.* **2017**, *15* (1), 79.
(69) Tsoi, K. M.; Dai, Q.; Alman, B. A.; Chan, W. C. W. Are Quantum Dots Toxic? Exploring the Discrepancy between Cell Culture and Animal Studies. *Acc. Chem. Res.* **2013**, *46* (3), 662−671.
(70) Choi, H. S.; Frangioni, J. V. Nanoparticles for Biomedical Imaging: Fundamentals of Clinical Translation. *Mol. Imaging* **2010**, *9* (6), 291−310.
(71) Fang, M.; Peng, C.-W.; Pang, D.-W.; Li, Y. Quantum Dots for Cancer Research: Current Status, Remaining Issues, and Future Perspectives. *Cancer Biol. Med.* **2012**, *9* (3), 151−163.
(72) Anselmo, A. C.; Mitragotri, S. A Review of Clinical Translation of Inorganic Nanoparticles. *AAPS J.* **2015**, *17* (5), 1041−1054.

https://dx.doi.org/10.1021/acs.nanolett.9b05259
Nano Lett. XXXX, XXX, XXX−XXX